ACS APPLIED MATERIALS & INTERFACES

www.acsami.org

Research Article

Triple Amplification of 3,4,9,10-Perylenetetracarboxylic Acid by Co^{2+}-Based Metal–Organic Frameworks and Silver–Cysteine and Its Potential Application for Ultrasensitive Assay of Procalcitonin

Xianzhen Song, Xinrong Shao, Li Dai,* Dawei Fan, Xiang Ren, Xiaojun Sun, Chuannan Luo,* and Qin Wei*

Cite This: *ACS Appl. Mater. Interfaces* 2020, 12, 9098–9106

Read Online

ACCESS | Metrics & More | Article Recommendations | Supporting Information

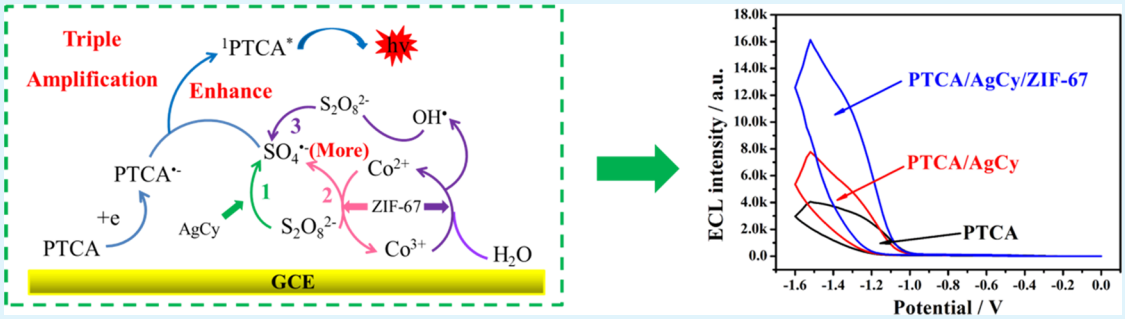

ABSTRACT: In this work, a triple-amplified biosensor with a bioactivity-maintained peculiarity was constructed for quantitative procalcitonin (PCT) detection. As everyone knows, a strong electrochemiluminescence (ECL) signal is the premise to ensure high sensitivity for trace target detection. Hence, a valid tactic was developed to achieve signal amplification of luminophor by using Co^{2+}-based metal–organic frameworks (ZIF-67) and silver–cysteine (AgCys). The ZIF-67 particles, which have more atomically dispersed Co^{2+}, could play the role of a co-reaction accelerator to catalyze $S_2O_8^{2-}$ to generate abundant Co^{3+} and sulfate radical anions ($SO_4^{\bullet-}$). Afterward, a mass of Co^{3+} was reduced to more hydroxyl radicals ($OH^{\bullet}$) by H_2O, thus ulteriorly reducing $S_2O_8^{2-}$ to generate more $SO_4^{\bullet-}$. Remarkably, $S_2O_8^{2-}$ was reduced to $SO_4^{\bullet-}$ continuously with the recycling of Co^{2+} and Co^{3+}, which realized an effective signal amplification. Meanwhile, the AgCys complex with superior catalysis and biocompatibility was prepared to further improve the ECL signal and maintain the bioactivity of the biomolecule. Furthermore, HWRGWVC, a heptapeptide that was used for combining the Fc fragments of an antibody by Au–S bonding to achieve the fixed point fixation, could not only maintain bioactivity of an antibody but also improved its incubation efficiency, thus further enhancing biosensor sensitivity. Under optimum conditions, the proposed biosensor realized highly sensitive assay for PCT with a wide dynamic range from 10 fg/mL to 100 ng/mL and a detection limit as low as 3.67 fg/mL. With superior stability, selectivity, and repeatability, the prepared biosensor revealed immense potential application of ultrasensitive assay for PCT in human serum.

KEYWORDS: *biosensor, procalcitonin, signal amplification, ZIF-67, co-reaction accelerator*

1. INTRODUCTION

Procalcitonin (PCT), which is normally secreted via thyroid C cells, reflects the activity of systemic inflammatory response.[1] Furthermore, with the occurrence of serious bacterial infection, multiple organ failure, and sepsis, the concentration of PCT in plasma increased.[2] Therefore, PCT could serve as an important indicator for the monitoring and diagnosis of systemic inflammatory response. So far, only a few analytical means have been reported for quantitative detection of PCT, such as chemiluminescence immunoassay,[3] surface plasmon resonance,[4] and fluorescence analysis.[5] Hence, it is essential to exploit a fast and highly efficient detection means to realize ultrasensitive assay for PCT.

Electrochemiluminescence (ECL), a light-emission progress that is produced by excited luminescent materials, has become one of the most important electrochemical detection means in various domains.[6−9] Up to now, ECL has attracted extensive attention on account of its high sensitivity, wide linear range, excellent controllability, and rapidness.[10,11] 3,4,9,10-Perylenetetracarboxylic acid (PTCA), a five-ring aromatic hydrocarbon with a large number of carboxyl groups, has extensive

Received: December 24, 2019
Accepted: January 28, 2020
Published: January 28, 2020

https://dx.doi.org/10.1021/acsami.9b23248
ACS Appl. Mater. Interfaces 2020, 12, 9098–9106

Scheme 1. Schematic Diagram of the (A) Preparation Step of Ab_2-Au-PTCA@ZIF-67 Bioconjugates and (B) Fabrication Procedure of the Biosensor

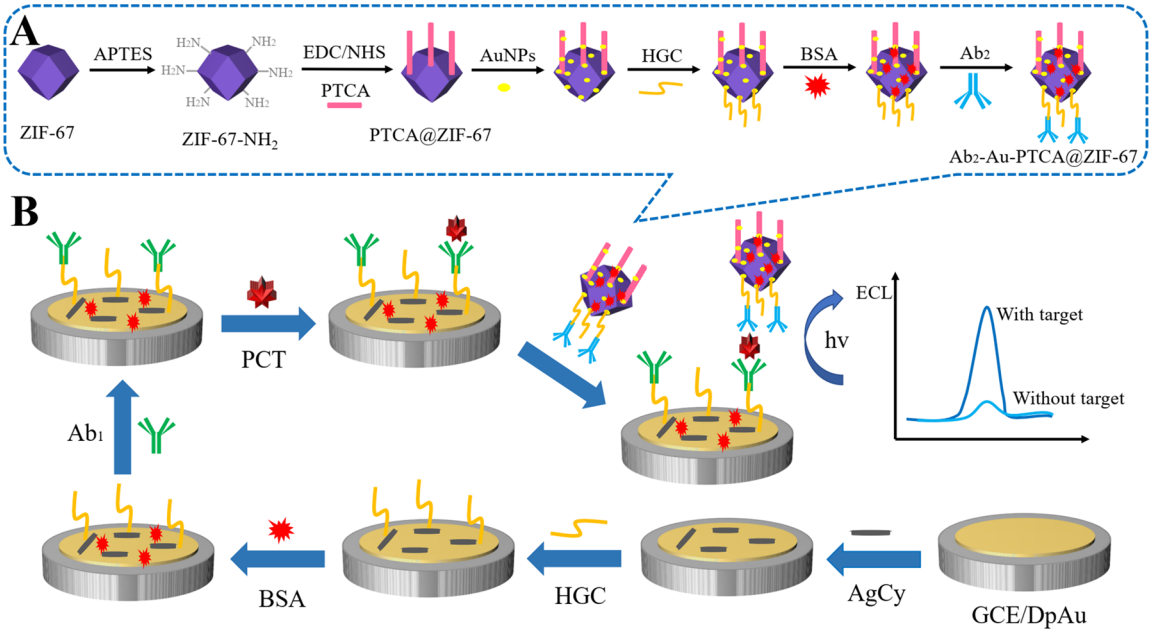

applications in ECL research because of its stable ECL emission in $S_2O_8^{2-}$ solution.[12] Furthermore, PTCA has a high specific surface area and superior conductivity property, which indicated that it could serve as luminophor to construct a sensing platform. Nevertheless, PTCA itself could not generate enough ECL emission to meet the demands of trace analysis, which prompted us to find an effective enhancer to improve its ECL signal.

Metal−organic frameworks (MOFs), which have excellent chemical and physical performance, such as polymetallic sites, porous structures, and high specific surface areas, are made up of metal ions and organic ligands.[13,14] Specifically, polymetallic sites are the key to improve catalytic performance; whereas, the porous structure can make full use of these atomically dispersed metal sites. Hence, MOFs have superior catalytic activity, which display extensive applications in the field of catalysis.[15,16] At present, some researchers have used MOFs as catalysts to promote ECL emission.[17,18] A silver−cysteine (AgCys) complex is a novel protein-like hybrid nanomaterial that has high catalytic activity and excellent biocompatibility.[19] Therefore, it can catalyze a co-reactant to produce more reactive intermediate states, thus amplifying the ECL signal. Furthermore, it can protect the bioactivity of the biosensor compared with pure AgNPs. Herein, we used Co^{2+}-based MOFs (ZIF-67) and AgCys to realize efficient catalysis of $S_2O_8^{2-}$, thus greatly enhancing the ECL emission of PTCA.

In this work, a triple amplification tactic was designed to achieve an effective enhancement for ECL behavior of luminophor in a PTCA−$S_2O_8^{2-}$ system. First of all, ZIF-67 was aminated via (3-aminopropyl)triethoxysilane (APTES). Afterward, the carboxyl activated PTCA was combined to the functionalized ZIF-67 via a condensation reaction between amino and carboxyl, and the PTCA@ZIF-67 complex was obtained as a signal probe. The ZIF-67 particles, which have more atomically dispersed Co^{2+} and large specific surface areas, not only serve as a co-reaction accelerator but also combine more PTCA, thereby greatly enhancing the ECL signal. Concretely, Co^{2+} could first reduce $S_2O_8^{2-}$ to generate abundant Co^{3+} and $SO_4^{\bullet-}$. After that, the acquired Co^{3+} was reduced to generate plentiful $OH^{\bullet}$ by H_2O, thus ulteriorly reducing $S_2O_8^{2-}$ to obtain more $SO_4^{\bullet-}$. Remarkably, $S_2O_8^{2-}$ was reduced to $SO_4^{\bullet-}$ in succession with the cyclic reaction between Co^{2+} and Co^{3+}, which realized an effective signal amplification. Meanwhile, the AgCys complex was synthesized to catalyze $S_2O_8^{2-}$ to produce more $SO_4^{\bullet-}$, thus amplifying the ECL signal once again. Furthermore, HWRGWVC (HGC), a heptapeptide with many advantages, such as low cost, simple preparation, and excellent stability, was introduced into the biosensor, which could combine the Fc fragments of an antibody by Au−S bonding to achieve the fixed point fixation.[20] Meanwhile, the incubation efficiency of the antibody was improved with the introduction of HGC, which enhanced the sensitivity of the biosensor. With superior sensitivity and bioactivity, the proposed triple-amplified biosensor realized an ultrasensitive assay of PCT in human serum.

2. EXPERIMENTAL SECTION

2.1. Synthesis of AgCys Complex. The AgCys complex was prepared on the basis of a previous research study.[21] In brief, 1 mL of cysteine and 2 mL of $AgNO_3$ solution were first mixed with magnetic stirring for 1 h. Afterward, the mixture was heated to 80 °C and reacted at this temperature for 40 min to obtain the white precipitate. At last, the AgCys complex was acquired by centrifuging and washing.

2.2. Preparation of Ab_2 Bioconjugates (Ab_2-Au-PTCA@ZIF-67). The synthesis of PTCA and ZIF-67 was carried out according to previous papers,[22,23] and the particular preparation procedure is shown in the Supporting Information. First, the as-prepared ZIF-67 was dissolved in toluene, and then 1 mL of APTES was added to it with ultrasonication for 50 min. After that, the mixed solution was moved to a Teflon-lined autoclave, reacting at 90 °C for 24 h, and ZIF-67-NH_2 was obtained. Next, 2 mL of a solution containing EDC (40 mM) and NHS (10 mM) was added to 5 mL of PTCA solution, reacting at 4 °C for 1 h, and then reacted with 5 mL of ZIF-67-NH_2 solution. Afterward, 1 mL of $HAuCl_4$ solution (1%) was added into it to obtain PTCA-Au@ZIF-67, and then it was dissolved in phosphate-buffered saline (PBS, pH 7.4) for further use. Finally, HGC, BSA, and Ab_2 were mixed with the above solution successively, and Ab_2 bioconjugates were prepared successfully after incubating it at 4 °C for 12 h.

https://dx.doi.org/10.1021/acsami.9b23248
ACS Appl. Mater. Interfaces 2020, 12, 9098−9106

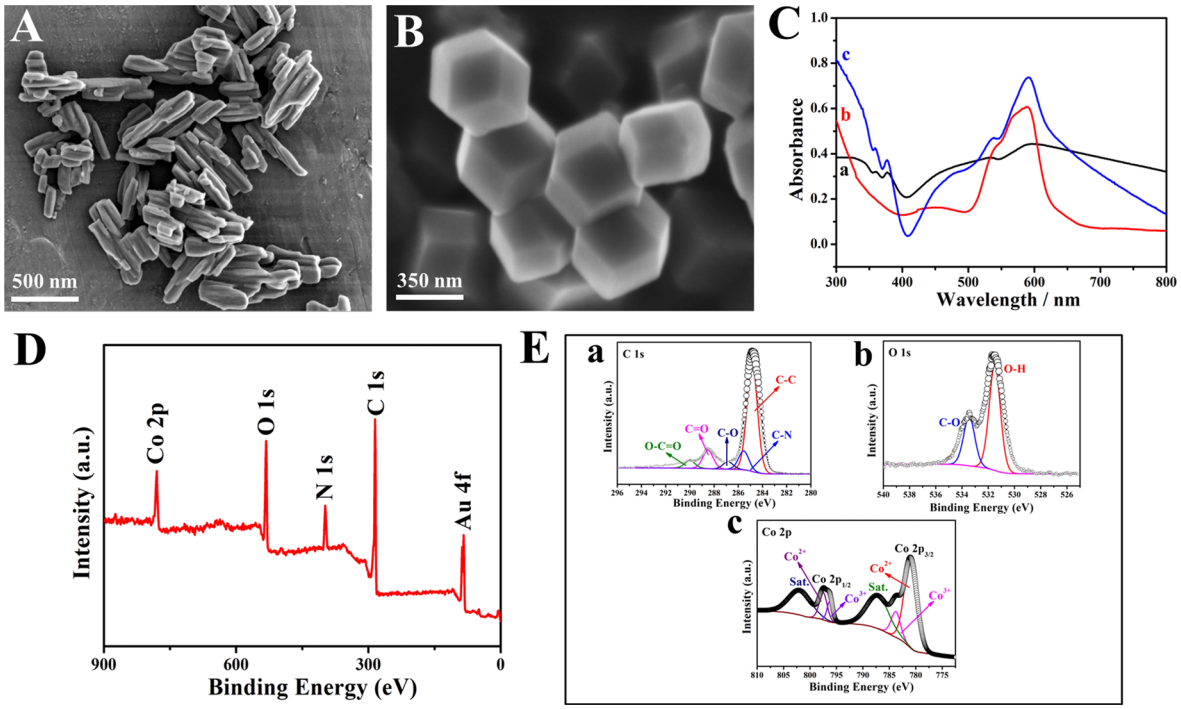

Figure 1. SEM images of (A) PTCA and (B) ZIF-67. (C) UV−vis spectra of (a) PTCA, (b) ZIF-67, and (c) PTCA-Au@ZIF-67. (D) Entire region of XPS spectrum for PTCA-Au@ZIF-67. (E) Different elements of (a) C 1s (b) O 1s, and (c) Co 2p regions.

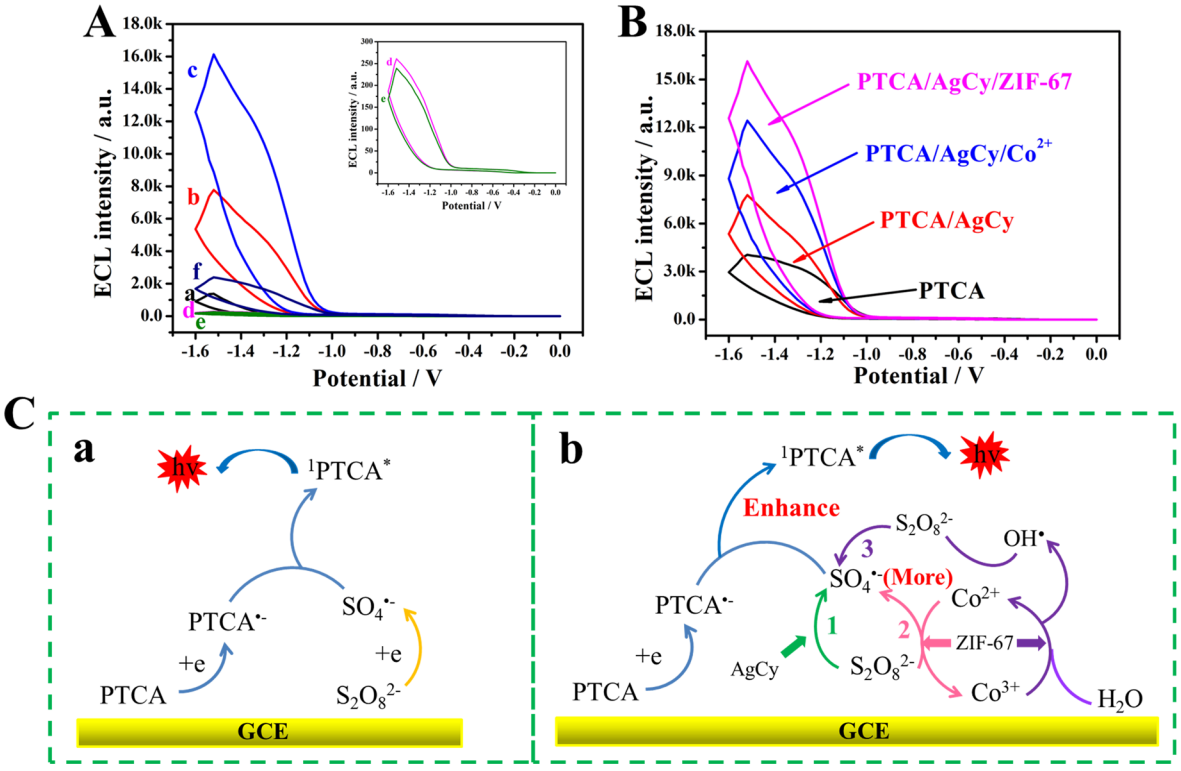

Figure 2. (A) ECL intensity−potential curves of various systems of (a) bare GCE, (b) PTCA/GCE, (c) PTCA/AgCys/ZIF-67/GCE, and (f) AgCys/ZIF-67/GCE in $S_2O_8^{2-}$ solution and (d) PTCA/AgCys/ZIF-67/GCE and (e) PTCA/GCE in PBS. (B) ECL intensity−potential curves of PTCA/GCE, PTCA/AgCys/GCE, PTCA/AgCys/Co^{2+}/GCE, and PTCA/AgCys/ZIF-67/GCE in $S_2O_8^{2-}$ solution. (C) Schematic diagram of a possible ECL mechanism in PTCA−$S_2O_8^{2-}$ system (a) without and (b) with AgCys/ZIF-67.

2.3. Fabrication of ECL Biosensor. Scheme 1 exhibits the detailed fabrication procedure of the ECL biosensor. First, the glassy carbon electrode (GCE) was polished with 0.3 and 0.05 μm Al_2O_3 slurries in sequence to acquire a mirror-like surface. Second, the as-prepared electrode was immersed in a solution of $HAuCl_4$ (1%) to obtain a thin tier of AuNPs by electrochemical deposition. After drying, the prepared AgCys solution was dropped on the electrode surface, and then the modified electrode was immersed in HGC solution (50 ng/mL) for 2 h

https://dx.doi.org/10.1021/acsami.9b23248
ACS Appl. Mater. Interfaces 2020, 12, 9098−9106

to bind it via Au−S bonding. After that, the electrode was immersed in Ab_1 (10 μg/mL) and BSA (1%) in sequence. Next, 10 μL of various concentrations of PCT was dispersed on the electrode surface with incubation at 4 °C for 1 h. At last, 10 μL of Ab_2 bioconjugates was dispersed on the electrode surface and incubation was carried out at 4 °C.

3. RESULTS AND DISCUSSION

3.1. Characterization of Nanomaterials. The morphologies and sizes of prepared nanomaterials were investigated by scanning electron microscopy (SEM). As shown in Figure 1A, PTCA exhibited a distinct short rod-like structure with a length of ∼500 nm, owing to hydrogen bonding and π−π stacking.[24] Meanwhile, ZIF-67 particles exhibited a dodecahedron structure with side lengths of ∼350 nm (Figure 1B), which was similar to previous papers.[23] Besides, UV characterization was carried out to prove successful synthesis of PTCA-Au@ZIF-67. As illustrated in Figure 1C, PTCA displayed three absorption peaks that were related to π−π* transitions between aromatic groups (curve a).[25] Curve b exhibited three absorption peaks of ZIF-67 at 588, 566, and 542 nm, which were regarded as the spin coupling triplet peaks.[26] According to curve c, the absorption peaks of PTCA-Au@ZIF-67 at 591 nm became wider, which was because of the cross-linking effect between PTCA and ZIF-67. Besides, there was a new absorption peak that appeared at 528 nm due to the combination of AuNPs. Hence, we believed that the PTCA-Au@ZIF-67 was prepared successfully.

To further prove the integrated preparation of PTCA-Au@ZIF-67, the XRD patterns of PTCA, ZIF-67, and PTCA-Au@ZIF-67 were studied. As shown in Figure S1A, there were four peaks that were indexed at 12.8° (111), 16.6° (010), 22.3° (102), and 27.4° (201) (curve b), and the results were in conformity to previous research.[27] Furthermore, the XRD patterns (Figure S1B) exhibited six characteristic peaks that were indexed to ZIF-67 (CCDC no. 1429244). Thus, the PTCA and ZIF-67 were successfully synthesized. Remarkably, PTCA-Au@ZIF-67 exhibited nearly identical peaks as PTCA, ZIF-67, and AuNPs (curve c), which indicated its successful synthesis.

The XPS characterization was presented to study the chemical composition of PTCA-Au@ZIF-67 through elemental analysis. According to Figure 1D, the peaks of Co 2p, O 1s, N 1s, C 1s, and Au 4f all appeared in PTCA-Au@ZIF-67. As illustrated in Figure 1E, the XPS spectra of C 1s region split in four peaks at 284.8, 286.4, 288.5, and 289.7 eV (panel a), which could be attributed to C−C (284.8 eV), C−O (286.4 eV), C═O (288.5 eV), and O−C═O (289.7 eV) bonds, respectively.[28] Besides, the spectra of the O 1s region was on account of O−H (531.5 eV) and C−O (533.4 eV) bonds (panel b), which may correspond to the carboxyl in PTCA.[29] The high-resolution Co 2p spectra (panel c) displayed two chief peaks at 797.5 and 781.1 eV, which were in line with Co^{2+} and Co^{3+}, respectively. Meanwhile, there were another two peaks at 787.4 and 802.1 eV, which could be regarded as shake up satellites. The above analyses proved that Co^{2+} was the primary valence state in the ZIF-67 phase.[30,31] Therefore, we could deduce that PTCA-Au@ZIF-67 was successfully prepared through the elemental analysis results.

3.2. Possible ECL Mechanism for Triple Amplification Tactic. To study a possible ECL enhancing mechanism of ZIF-67 particles and the AgCys complex, the ECL responses in various systems were measured. As illustrated in Figure 2A, the ECL peak of bare GCE was first detected in $S_2O_8^{2-}$ solution, which was because of the emission of singlet oxygen ($^1(O_2)_2$*) (curve a).[32] Curve b demonstrated the ECL response of pure PTCA, which was ascribed to the emission of the PTCA excited state (^{1}PTCA*).[33] Afterward, a further modified electrode, PTCA/ZIF-67/AgCys/GCE, was tested in a $S_2O_8^{2-}$ solution, and the results exhibited a significant enhancement of ECL intensity compared to pure PTCA (curve c). This was due to the fact that the combined use of ZIF-67 particles and AgCys complex could catalyze $S_2O_8^{2-}$ to generate more $SO_4^{\bullet-}$, thus effectively improving the ECL response. To further verify the enhancing mechanism, the modified electrode (PTCA/ZIF-67/AgCys/GCE) was tested in PBS, and the result indicated that there was almost no ECL peak (curve d), which was similar to the ECL response of pure PTCA in a PBS solution (curve e). Therefore, we could infer that ZIF-67 particles and the AgCys complex could not directly react with PTCA to realize the ECL signal amplification. Finally, a modified electrode, AgCys/ZIF-67/GCE, was detected in a $S_2O_8^{2-}$ solution (curve f). More interestingly, curve f exhibited a distinct signal enhancement compared with curve a, which further proved that ZIF-67 particles and the AgCys complex could catalyze $S_2O_8^{2-}$ to generate a mass of $SO_4^{\bullet-}$, thereby realizing an effective emission of $^1(O_2)_2$*.

To explore the enhanced effectiveness of ZIF-67 particles and the AgCys complex on PTCA, the ECL responses of PTCA, PTCA-AgCys, PTCA-AgCys@ZIF-67, and PTCA-AgCys with free Co^{2+} were measured. There was an obvious improvement in the ECL signal of PTCA-AgCys, which was twice as much as that of pure PTCA (Figure 2B). After continuing to modify the electrode with ZIF-67, the ECL signal was further enhanced to 16,100 au, which was approximately 8300 au more than that of PTCA-AgCys. Furthermore, the ECL response of PTCA-AgCys with the addition of Co^{2+} was obtained, and the concentrations of Co^{2+} and ZIF-67 were the same. The result indicated that the enhanced effectiveness of ZIF-67 was stronger than that of free Co^{2+}. Hence, an effective ECL enhancement by ZIF-67 may be attributed to its ordered porous crystal structure and more atomically dispersed Co^{2+}, which could promote the reduction of $S_2O_8^{2-}$. Furthermore, the large specific surface area of ZIF-67 could provide an excellent platform to combine more luminophor.

The possible ECL mechanism is described in detail in Figure 2C. First of all, $PTCA^{\bullet-}$ was generated with the reduction of PTCA, and then it reacted with $SO_4^{\bullet-}$ (less) to obtain little ^{1}PTCA* for a low ECL emission (a). After the AgCys complex and ZIF-67 particles were introduced in the reaction system, the production of $SO_4^{\bullet-}$ notably increased, which realized the triple signal amplification (b). In route 1, the AgCys complex catalyzed $S_2O_8^{2-}$ to generate more $SO_4^{\bullet-}$, thus enhancing the ECL signal (eq 1). In route 2, the Co^{2+} reacted with $S_2O_8^{2-}$ to generate abundant $SO_4^{\bullet-}$ and Co^{3+} (eq 2). Furthermore, the acquired Co^{3+} could be reduced via H_2O to produce a mass of Co^{2+} and $OH^{\bullet}$, thus further reducing $S_2O_8^{2-}$ to generate more $SO_4^{\bullet-}$ (route 3, eqs 3−6). Importantly, the cyclic reaction between Co^{2+} and Co^{3+} could produce $SO_4^{\bullet-}$ continuously, which effectively amplified the ECL signal. In summary, a possible mechanism of the proposed biosensor is shown in eqs 1−9.

Route 1:

$$S_2O_8^{2-} + e^- \xrightarrow{AgCys} SO_4^{2-}SO_4^{\cdot-}(more) \quad (1)$$

Route 2:

https://dx.doi.org/10.1021/acsami.9b23248
ACS Appl. Mater. Interfaces 2020, 12, 9098−9106

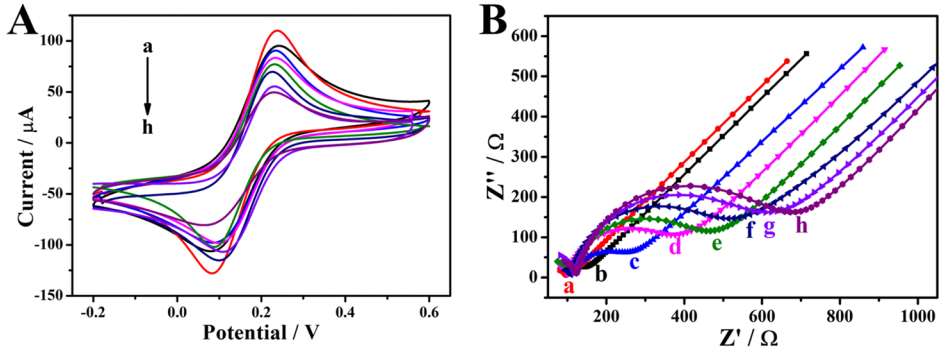

Figure 3. (A) CV and (B) EIS profiles of stepwise-modified electrodes in a 0.1 M PBS solution containing 0.1 M KCl and 5 mM $Fe(CN)_6^{3-/4-}$: (a) DpAu/GCE, (b) bare GCE, (c) DpAu/AgCys/GCE, (d) DpAu/AgCys/HGC/GCE, (e) DpAu/AgCys/HGC/Ab_1/GCE, (f) DpAu/AgCys/HGC/Ab_1/BSA/GCE, (g) DpAu/AgCys/HGC/Ab_1/BSA/PCT/GCE, and (h) DpAu/AgCys/HGC/Ab_1/BSA/PCT/Ab_2-Au-PTCA@ZIF-67/GCE.

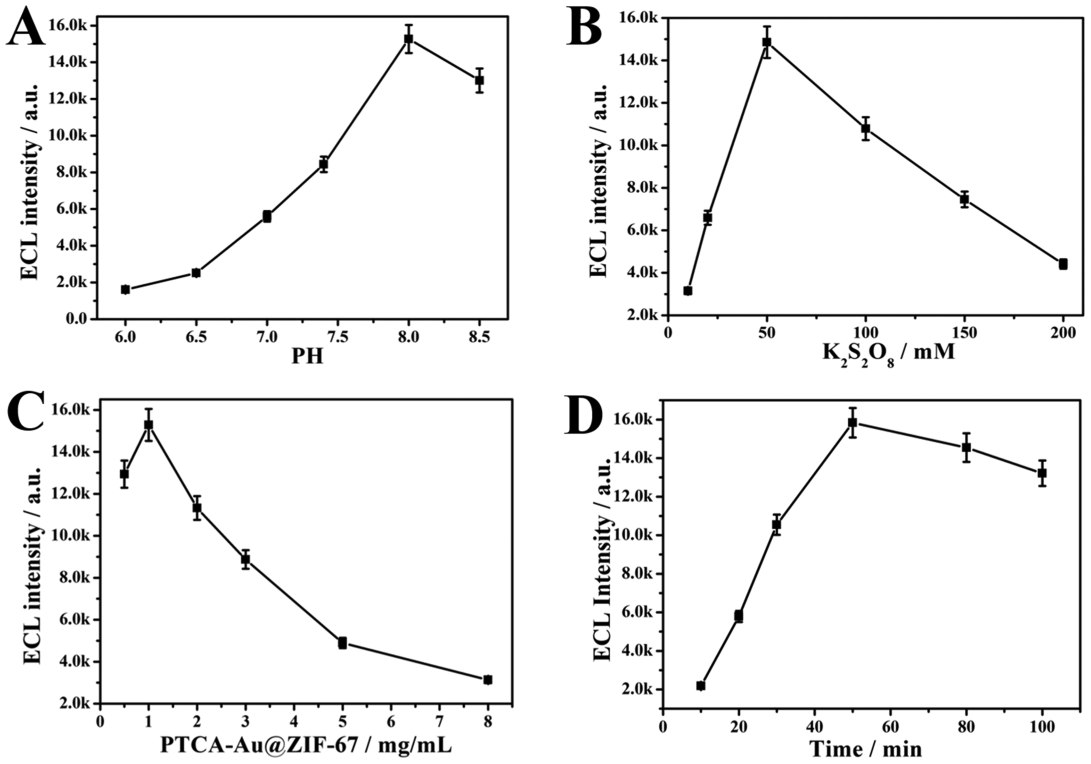

Figure 4. Optimization of (A) pH value, (B) $K_2S_2O_8$ concentration, (C) PTCA-Au@ZIF-67 concentration, and (D) incubation time of Ab_2.

$$Co^{2+} + S_2O_8^{2-} \rightarrow Co^{3+} + SO_4^{2-} + SO_4^{\cdot -} \quad (2)$$

Route 3:

$$4Co^{3+} + 2H_2O \rightarrow 4Co^{2+} + 4H^+ + O_2 \quad (3)$$

$$O_2 + H_2O + e^- \rightarrow OH^- + H_2O_2 \quad (4)$$

$$H_2O_2 + e^- \rightarrow OH^- + OH^{\cdot} \quad (5)$$

$$OH^{\cdot} + S_2O_8^{2-} \rightarrow HSO_4^- + O_2 + SO_4^{\cdot -} \quad (6)$$

ECL emission:

$$PTCA + e^- \rightarrow PTCA^{\cdot -} \quad (7)$$

$$PTCA^{\cdot -} + SO_4^{\cdot -} \rightarrow {}^1PTCA^* + SO_4^{2-} \quad (8)$$

$$^1PTCA^* \rightarrow PTCA + h\nu \quad (9)$$

3.3. Electrochemical Characterizations of the Biosensor. The stepwise characterization of the prepared biosensor was achieved via cyclic voltammetry (CV) measurement, and relevant results are exhibited in Figure 3A, which proved its successful fabrication. First, the quasi-reversible redox peak was acquired with a measurement of the bare GCE (curve b). After modifying it with AuNPs, GCE/DpAu exhibited an increased current peak compared to a bare electrode because of promotion of the electron transfer by AuNPs (curve a). The current peak was reduced after the AgCys solution was dropped on the modified electrode, owing to its obstruction for electron transfer (curve c). After that, the current peak further decreased with the successive modification of HGC, Ab_1, BSA, and PCT, which was because of the electric insulativity of these biomolecules (curves d, e, f, and g). Finally, the current peak decreased again with the modification of the Ab_2 bioconjugates (curve h). The above results revealed that the proposed biosensor was fabricated successfully.

https://dx.doi.org/10.1021/acsami.9b23248
ACS Appl. Mater. Interfaces 2020, 12, 9098−9106

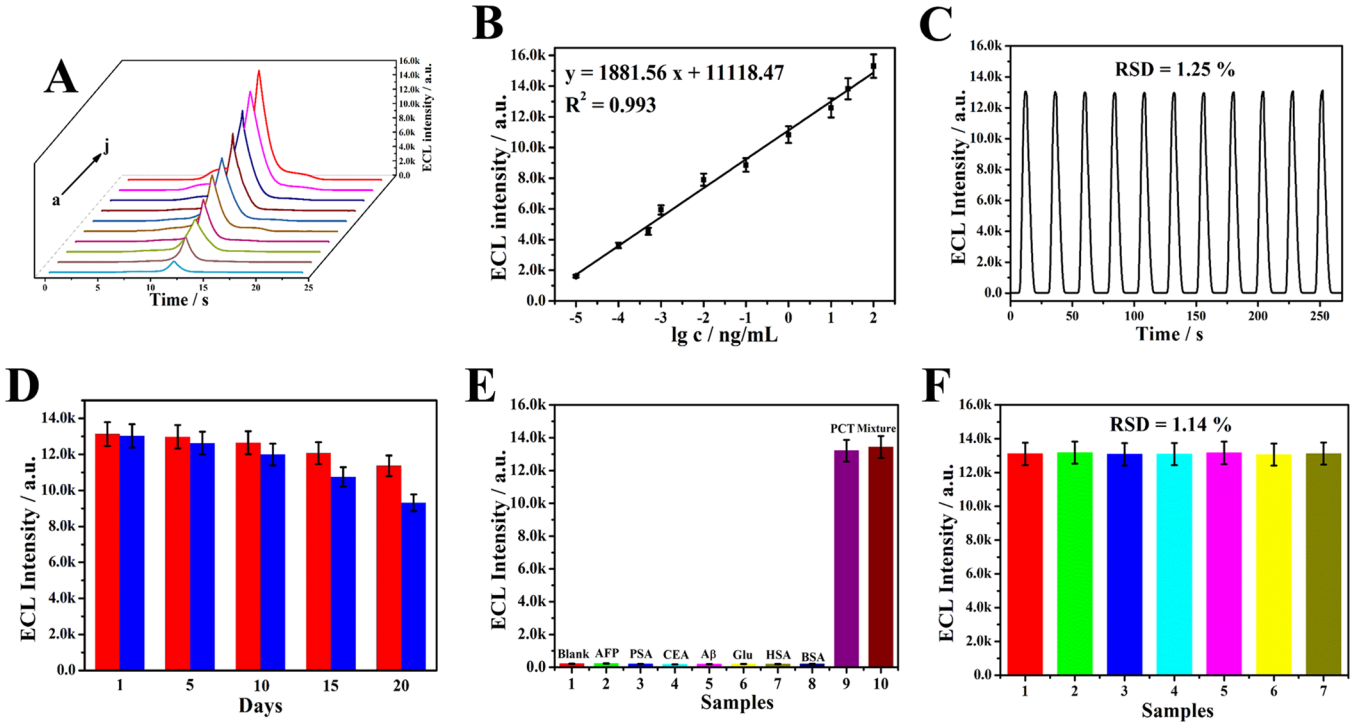

Figure 5. (A) ECL intensity−time curves and (B) correlative calibration curve of the biosensor detected with various PCT concentrations in a 50 mM $S_2O_8^{2-}$ solution: (a) 10 fg/mL, (b) 100 fg/mL, (c) 500 fg/mL, (d) 1 pg/mL, (e) 10 pg/mL, (f) 100 pg/mL, (g) 1 ng/mL, (h) 10 ng/mL, (i) 50 ng/mL, and (j) 100 ng/mL. (C) Operation stability of the prepared biosensor under continuous potential scanning (11 scans). (D) Storage stability of the proposed biosensor. (E) Selectivity of the proposed biosensor to different targets. (F) Repeatability of the biosensor under the detection of seven different electrodes.

Furthermore, the successful preparation of biosensor could be also confirmed by EIS characterization of the stepwise-modified electrode. The EIS curve of bare electrode showed a small semicircle, and the related results are displayed in Figure 3B, which was attributed to the free-electron transfer (curve b). Comparing to the bare electrode, the curve of GCE/DpAu exhibited a smaller semicircle because of the superior conductivity of AuNPs (curve a). After AgCys was covered on the surface of the modified electrode, the semicircle increased because of an impediment of electron transfer by it (curve c). Afterward, with the successive modification by HGC, Ab_1, BSA, and PCT, the resistance increased in sequence (curves d, e, f, and g). After that, the resistance further increased with the final modification of Ab_2 bioconjugates (curve h). Therefore, it was confirmed that the biosensor was successfully fabricated according to the above results.

3.4. Optimization of Experimental Conditions. To gain better experimental results, the experimental conditions were optimized. As illustrated in Figure 4A, there was a distinct enhancement in the ECL signal with an increase in pH value from 6.0 to 8.0, which may be ascribed to the suppression of luminescence due to rapid reduction of proton at low pH. Afterward, the ECL intensity began to reduce because of the impact on biological activity of PCT at high pH. Therefore, the optimal pH was at 8.0. The optimization of the concentration of $K_2S_2O_8$ is shown in Figure 4B, which exhibited that the ECL intensity reached a maximum at 50 mM. The reason for the reduction of the ECL signal may be an inhibition for the production of ^{1}PTCA* in superabundant $S_2O_8^{2-}$.[34] Meanwhile, excess $S_2O_8^{2-}$ also affected the biological activity of PCT. Hence, 50 mM was selected as the optimal concentration of $K_2S_2O_8$. As illustrated in Figure 4C, a maximum of the ECL signal appeared when the PTCA-Au@ZIF-67 concentration reached 1 mg/mL, which may be due to the self-absorption effect of luminophor,[35] thereby reducing the ECL signal in high PTCA-Au@ZIF-67 concentration. In consequence, the optimal PTCA-Au@ZIF-67 concentration was at 1 mg/mL. Finally, the optimization of the incubation time for Ab_2 bioconjugates is shown in Figure 4D, and the result displayed an optimal incubation time at 50 min. Furthermore, the incubation time for Ab_2 bioconjugates was shorter than those of usual methods, which was ascribed to the site-oriented immobilization of the antibody by HGC, thus immensely improving its incubation efficiency.

3.5. ECL Responses of the Proposed Biosensor to PCT. In this study, the ECL responses of the biosensor toward different PCT concentrations were obtained under optimal conditions. As shown in Figure 5A, the ECL signal enhanced successively when the PCT concentration was increased from 10 fg/mL to 100 ng/mL. In addition, Figure 5B reveals the related linear relationship of ECL intensity (I) and logarithm of PCT concentration (lgc), with a linear equation of I = 1881.56 lgc + 11118.47 and a correlation coefficient of 0.993. Therefore, the prepared biosensor revealed a wide linear range from 10 fg/mL to 100 ng/mL and a detection limit as low as 3.67 fg/mL, which had higher sensitivity than those in previous papers (Table 1). The results proved that the proposed biosensor achieved an ultrasensitive PCT detection.

3.6. Stability, Selectivity, and Repeatability of the Proposed Biosensor. Stability is an important index to assess biosensor performance. Figure 5C exhibits the superior operation stability with a low relative standard deviation (RSD) of 1.25% for PCT detection under 11 cycles of continuous potential scanning. Meanwhile, the storage stability

https://dx.doi.org/10.1021/acsami.9b23248
ACS Appl. Mater. Interfaces 2020, 12, 9098−9106

Table 1. Comparison of the Proposed Biosensor with Previous Papers for PCT Assay

methods	linear range (ng/mL)	detection limit (pg/mL)	references
imaging ellipsometry	0.13−128	81	2
CLIA	0.0025−80	0.5	3
SPR	20−4000	9.9	4
electrochemical	0.0018−500	0.36	36
microfluidic	0.25−128	43.9	37
ECL	0.01−20	3.4	38
ECL	0.0005−100	0.18	39
ECL	0.0001−50	0.054	40
ECL	0.00001−100	0.0037	this work

of the biosensor was investigated via ECL responses for different storage times at 4 °C. As illustrated in Figure 5D, after 20 days, the ECL signal of the proposed biosensor was reduced around 13.4% (red), which was better than the biosensor without HGC (blue). The results revealed that the storage stability became better with the introduction of HGC, which proved that it effectively maintained bioactivity of the biosensor. In short, the proposed biosensor exhibited an excellent stability.

To assess the selectivity of the biosensor, alpha-fetoprotein, prostate-specific antigen, carcinoembryonic antigen, amyloid-β protein, glucose, serum albumin, and bovine serum albumin (BSA) were used as the interferences. As shown in Figure 5E, the ECL responses of interferences (10 ng/mL) were almost the same as the blank sample. Meanwhile, the ECL intensity of PCT (1 ng/mL) was very close to that of the mixed sample (containing 1 ng/mL PCT and 10 ng/mL interferences), which exhibited an excellent selectivity of the proposed biosensor. Besides, the repeatability of the prepared biosensor was studied via ECL responses of seven various electrodes. As shown in Figure 5F, there was no evident difference between the ECL intensity of seven electrodes with a low RSD of 1.14%, which proved a great repeatability of the proposed biosensor.

3.7. Analysis of Real Samples. In this study, the human serum samples were supplied without any purification treatment to verify the feasibility of the biosensor in real sample analysis. Besides, different concentrations of targets were added to the diluted serum samples (0.32, 2.81, and 4.66 ng/mL) for testing. As described in Table S1, the recovery rate ranging from 99.6% to 100.4% was acquired by the standard addition method, which indicated a great accuracy of the biosensor. In addition, the RSD of the proposed biosensor was in the range of 1.05−1.14%, which verified its excellent precision. Hence, we believed that the proposed biosensor was suitable for ultrasensitive assay for PCT in real samples.

4. CONCLUSIONS

In summary, an effective triple amplification tactic was developed for ultrasensitive assay of PCT. With a large specific surface area, ordered crystal structure, and more atomically dispersed Co^{2+}, ZIF-67 could be utilized as the co-reaction accelerator to realize a strong signal amplification so as to markedly improve the sensitivity of the proposed biosensor. Because of the superior catalysis and biocompatibility, the prepared AgCys complex could further amplify the ECL signal and maintain the bioactivity of the biosensor. In addition, HGC was used to achieve the site-oriented fixation via the combination of the Fc fragments of an antibody, which protected the bioactivity of the antibody and enhanced its incubation efficiency. Therefore, a triple-amplified biosensor with a bioactivity-maintained peculiarity was constructed for an ultrasensitive assay of PCT with a wide dynamic range and an extremely low detection limit, which indicated its huge potential for the biomarker detection. Importantly, this work revealed the feasibility for the application of MOFs as a co-reaction accelerator to catalyze the co-reactant to produce more reactive intermediate species in the ECL field, which indicated that it is coming within reach to push ECL detection sensitivity to hypersensitive bioassay.

■ ASSOCIATED CONTENT

Supporting Information

The Supporting Information is available free of charge at https://pubs.acs.org/doi/10.1021/acsami.9b23248.

Experimental section, XRD patterns of PTCA-Au@ZIF-67, and analytical application of the biosensor in human serum samples (PDF)

■ AUTHOR INFORMATION

Corresponding Authors

Li Dai − *Collaborative Innovation Center for Green Chemical Manufacturing and Accurate Detection, Key Laboratory of Chemical Sensing & Analysis in Universities of Shandong, School of Chemistry and Chemical Engineering, University of Jinan, Jinan 250022, P. R. China*; Email: 18906404295@163.com

Chuannan Luo − *Collaborative Innovation Center for Green Chemical Manufacturing and Accurate Detection, Key Laboratory of Chemical Sensing & Analysis in Universities of Shandong, School of Chemistry and Chemical Engineering, University of Jinan, Jinan 250022, P. R. China*; Email: chm_luocn@ujn.edu.cn

Qin Wei − *Collaborative Innovation Center for Green Chemical Manufacturing and Accurate Detection, Key Laboratory of Chemical Sensing & Analysis in Universities of Shandong, School of Chemistry and Chemical Engineering, University of Jinan, Jinan 250022, P. R. China*; orcid.org/0000-0002-3034-8046; Phone: +86 531 82765730; Email: sdjndxwq@163.com; Fax: +86 531 82765969

Authors

Xianzhen Song − *Collaborative Innovation Center for Green Chemical Manufacturing and Accurate Detection, Key Laboratory of Chemical Sensing & Analysis in Universities of Shandong, School of Chemistry and Chemical Engineering, University of Jinan, Jinan 250022, P. R. China*

Xinrong Shao − *Collaborative Innovation Center for Green Chemical Manufacturing and Accurate Detection, Key Laboratory of Chemical Sensing & Analysis in Universities of Shandong, School of Chemistry and Chemical Engineering, University of Jinan, Jinan 250022, P. R. China; School of Chemical Engineering, Shandong University of Technology, Zibo 255049, P.R. China*

Dawei Fan − *Collaborative Innovation Center for Green Chemical Manufacturing and Accurate Detection, Key Laboratory of Chemical Sensing & Analysis in Universities of Shandong, School of Chemistry and Chemical Engineering, University of Jinan, Jinan 250022, P. R. China*

Xiang Ren − *Collaborative Innovation Center for Green Chemical Manufacturing and Accurate Detection, Key Laboratory of Chemical Sensing & Analysis in Universities of Shandong, School*

https://dx.doi.org/10.1021/acsami.9b23248
ACS Appl. Mater. Interfaces 2020, 12, 9098−9106

of Chemistry and Chemical Engineering, University of Jinan, Jinan 250022, P. R. China

Xiaojun Sun − *Collaborative Innovation Center for Green Chemical Manufacturing and Accurate Detection, Key Laboratory of Chemical Sensing & Analysis in Universities of Shandong, School of Chemistry and Chemical Engineering, University of Jinan, Jinan 250022, P. R. China*

Complete contact information is available at: https://pubs.acs.org/10.1021/acsami.9b23248

Notes

The authors declare no competing financial interest.

■ ACKNOWLEDGMENTS

This study was supported by the National Key Scientific Instrument and Equipment Development Project of China (no. 21627809) and the National Natural Science Foundation of China (nos. 21575050 and 21777056).

■ REFERENCES

(1) Vincenzi, B.; Fioroni, I.; Pantano, F.; Angeletti, S.; Dicuonzo, G.; Zoccoli, A.; Santini, D.; Tonini, G. Procalcitonin as Diagnostic Marker of Infection in Solid Tumors Patients with Fever. *Sci. Rep.* **2016**, *6*, 28090−28095.

(2) Li, Y.; Liu, W.; Jin, G.; Niu, Y.; Chen, Y.; Xie, M. Label-Free Sandwich Imaging Ellipsometry Immunosensor for Serological Detection of Procalcitonin. *Anal. Chem.* **2018**, *90*, 8002−8010.

(3) Nie, R.; Xu, X.; Cui, X.; Chen, Y.; Yang, L. A Highly Sensitive Capillary-Based Immunosensor by Combining with Peroxidase Nanocomplex-Mediated Signal Amplification for Detection of Procalcitonin in Human Serum. *ACS Omega* **2019**, *4*, 6210−6217.

(4) Sener, G.; Ozgur, E.; Rad, A. Y.; Uzun, L.; Say, R.; Denizli, A. Rapid Real-Time Detection of Procalcitonin Using a Microcontact Imprinted Surface Plasmon Resonance Biosensor. *Analyst* **2013**, *138*, 6422−6428.

(5) Zhou, Y.; Shao, X.; Han, Y.; Zhang, H. Detection of Procalcitonin (PCT) Using the Double Antibody Sandwich Method Based on Fluorescence Resonance Energy Transfer between Upconversion Nanoparticles and Quantum Dots. *Anal. Methods* **2018**, *10*, 1015−1022.

(6) Liu, S.; Zhang, J.; Tu, W.; Bao, J.; Dai, Z. Using Ruthenium Polypyridyl Functionalized ZnO Mesocrystals and Gold Nanoparticle Dotted Graphene Composite for Biological Recognition and Electrochemiluminescence Biosensing. *Nanoscale* **2014**, *6*, 2419−2425.

(7) Xu, J.; Huang, P.; Qin, Y.; Jiang, D.; Chen, H. Y. Analysis of Intracellular Glucose at Single Cells Using Electrochemiluminescence Imaging. *Anal. Chem.* **2016**, *88*, 4609−4612.

(8) Yang, H. Y.; Wang, H. J.; Xiong, C. Y.; Chai, Y. Q.; Yuan, R. Intramolecular Self-Enhanced Nanochains Functionalized by an Electrochemiluminescence Reagent and Its Immunosensing Application for the Detection of Urinary β2-Microglobulin. *ACS Appl. Mater. Interfaces* **2017**, *9*, 36239−36246.

(9) Yang, L.; Jia, Y.; Wu, D.; Zhang, Y.; Ju, H.; Du, Y.; Ma, H.; Wei, Q. Synthesis and Application of CeO_2/SnS_2 Heterostructures as a Highly Efficient Coreaction Accelerator in the Luminol-Dissolved O_2 System for Ultrasensitive Biomarkers Immunoassay. *Anal. Chem.* **2019**, *91*, 14066−14073.

(10) Zhang, Y. Y.; Feng, Q. M.; Xu, J. J.; Chen, H. Y. Silver Nanoclusters for High-Efficiency Quenching of CdS Nanocrystal Electrochemiluminescence and Sensitive Detection of MicroRNA. *ACS Appl. Mater. Interfaces* **2015**, *7*, 26307−26314.

(11) Jia, Y.; Yang, L.; Feng, R.; Ma, H.; Fan, D.; Yan, T.; Feng, R.; Du, B.; Wei, Q. $MnCO_3$ as a New Electrochemiluminescence Emitter for Ultrasensitive Bioanalysis of β-Amyloid$_{1-42}$ Oligomers Based on Site-Directed Immobilization of Antibody. *ACS Appl. Mater. Interfaces* **2019**, *11*, 7157−7163.

(12) Song, X.; Li, X.; Wei, D.; Feng, R.; Yan, T.; Wang, Y.; Ren, X.; Du, B.; Ma, H.; Wei, Q. CuS as Co-Reaction Accelerator in PTCA-$K_2S_2O_8$ System for Enhancing Electrochemiluminescence Behavior of PTCA and Its Application in Detection of Amyloid-β Protein. *Biosens. Bioelectron.* **2019**, *126*, 222−229.

(13) Liang, Z.; Qu, C.; Xia, D.; Zou, R.; Xu, Q. Atomically Dispersed Metal Sites in MOF-Based Materials for Electrocatalytic and Photocatalytic Energy Conversion. *Angew. Chem., Int. Ed.* **2018**, *57*, 9604−9633.

(14) Yang, Q.; Xu, Q.; Jiang, H. L. Metal-Organic Frameworks Meet Metal Nanoparticles: Synergistic Effect for Enhanced Catalysis. *Chem. Soc. Rev.* **2017**, *46*, 4774−4808.

(15) Zhao, L.; Kuang, X.; Kuang, R.; Tong, L.; Liu, Z.; Hou, Y.; Sun, X.; Wang, Z.; Wei, Q. MOF-Based Supramolecule Helical Nanomaterials: Toward Highly Enantioselective Electrochemical Recognition of Penicillamine. *ACS Appl. Mater. Interfaces* **2019**, *12*, 1533−1538.

(16) Zhao, L.; Kuang, X.; Chen, C.; Sun, X.; Wang, Z.; Wei, Q. Boosting Electrocatalytic Nitrogen Fixation via Energy-Efficient Anodic Oxidation of Sodium Gluconate. *Chem. Commun.* **2019**, *55*, 10170−10173.

(17) Wang, S.; Zhao, Y.; Wang, M.; Li, H.; Saqib, M.; Ge, C.; Zhang, X.; Jin, Y. Enhancing Luminol Electrochemiluminescence by Combined Use of Cobalt-Based Metal Organic Frameworks and Silver Nanoparticles and Its Application in Ultrasensitive Detection of Cardiac Troponin I. *Anal. Chem.* **2019**, *91*, 3048−3054.

(18) Fang, Q.; Lin, Z.; Lu, F.; Chen, Y.; Huang, X.; Gao, W. A Sensitive Electrochemiluminescence Immunosensor for the Detection of PSA Based on CdWS Nanocrystals and Ag^+@UIO-66-NH_2 as a Novel Coreaction Accelerator. *Electrochim. Acta* **2019**, *302*, 207−215.

(19) Chen, W.; Zheng, L.; Wang, M.; Chi, Y.; Chen, G. Preparation of Protein-like Silver-Cysteine Hybrid Nanowires and Application in Ultrasensitive Immunoassay of Cancer Biomarker. *Anal. Chem.* **2013**, *85*, 9655−9663.

(20) Yang, L.; Fan, D.; Zhang, Y.; Ding, C.; Wu, D.; Wei, Q.; Ju, H. Ferritin-Based Electrochemiluminescence Nanosurface Energy Transfer System for Procalcitonin Detection Using HWRGWVC Heptapeptide for Site-oriented Antibody Immobilization. *Anal. Chem.* **2019**, *91*, 7145−7152.

(21) Wang, J. X.; Zhuo, Y.; Zhou, Y.; Wang, H. J.; Yuan, R.; Chai, Y. Q. Ceria Doped Zinc Oxide Nanoflowers Enhanced Luminol-Based Electrochemiluminescence Immunosensor for Amyloid-β Detection. *ACS Appl. Mater. Interfaces* **2016**, *8*, 12968−12975.

(22) Zhuo, Y.; Liao, N.; Chai, Y. Q.; Gui, G. F.; Zhao, M.; Han, J.; Xiang, Y.; Yuan, R. Ultrasensitive Apurinic/Apyrimidinic Endonuclease 1 Immunosensing Based on Self-Enhanced Electrochemiluminescence of a Ru (II) Complex. *Anal. Chem.* **2014**, *86*, 1053−1060.

(23) Dou, S.; Dong, C.-L.; Hu, Z.; Huang, Y.-C.; Chen, J.-l.; Tao, L.; Yan, D.; Chen, D.; Shen, S.; Chou, S.; Yang, S. Atomic-Scale CoOx Species in Metal-Organic Frameworks for Oxygen Evolution Reaction. *Adv. Funct. Mater.* **2017**, *27*, 1702546−1702553.

(24) Lei, Y. M.; Wen, R. X.; Zhou, J.; Chai, Y. Q.; Yuan, R.; Zhuo, Y. Silver Ions as Novel Coreaction Accelerator for Remarkably Enhanced Electrochemiluminescence in a PTCA−$S_2O_8^{2-}$System and Its Application in an Ultrasensitive Assay for Mercury Ions. *Anal. Chem.* **2018**, *90*, 6851−6858.

(25) Alessio, P.; Braunger, M. L.; Aroca, R. F.; de Almeida Olivati, C.; Constantino, C. J. L. Supramolecular Organization-Electrical Properties Relation in Nanometric Organic Films. *J. Phys. Chem. C* **2015**, *119*, 12055−12064.

(26) Qin, J.; Wang, S.; Wang, X. Visible-Light Reduction CO_2 with Dodecahedral Zeolitic Imidazolate Framework ZIF-67 as an Efficient Co-Catalyst. *Appl. Catal., B.* **2017**, *209*, 476−482.

(27) Li, F.; Yang, H.; Shan, C.; Zhang, Q.; Han, D.; Ivaska, A.; Niu, L. The Synthesis of Perylene-Coated Graphene Sheets Decorated with Au Nanoparticles and Its Electrocatalysis toward Oxygen Reduction. *J. Mater. Chem.* **2009**, *19*, 4022−4025.

(28) Zhao, K.; Liu, S.; Ye, G.; Gan, Q.; Zhou, Z.; He, Z. High-Yield Bottom-up Synthesis of 2D Metal-Organic Frameworks and Their

Derived Ultrathin Carbon Nanosheets for Energy Storage. *J. Mater. Chem. A* **2018**, *6*, 2166−2175.
(29) Cai, Z.; Xu, W.; Li, F.; Yao, Q.; Chen, X. Electropolymerization Fabrication of Co Phosphate Nanoparticles Encapsulated in N, P-Codoped Mesoporous Carbon Networks as a 3D Integrated Electrode for Full Water Splitting. *ACS Sustainable Chem. Eng.* **2016**, *5*, 571−579.
(30) Zhu, G.; Wen, H.; Ma, M.; Wang, W.; Yang, L.; Wang, L.; Shi, X.; Cheng, X.; Sun, X.; Yao, Y. A Self-Supported Hierarchical Co-MOF as a Supercapacitor Electrode with Ultrahigh Areal Capacitance and Excellent Rate Performance. *Chem. Commun.* **2018**, *54*, 10499−10502.
(31) Wei, Z.; Zhu, W.; Li, Y.; Ma, Y.; Wang, J.; Hu, N.; Suo, Y.; Wang, J. Conductive Leaflike Cobalt Metal-Organic Framework Nanoarray on Carbon Cloth as a Flexible and Versatile Anode toward Both Electrocatalytic Glucose and Water Oxidation. *Inorg. Chem.* **2018**, *57*, 8422−8428.
(32) Ma, M. N.; Zhuo, Y.; Yuan, R.; Chai, Y. Q. New Signal Amplification Strategy Using Semicarbazide as Co-Reaction Accelerator for Highly Sensitive Electrochemiluminescent Aptasensor Construction. *Anal. Chem.* **2015**, *87*, 11389−11397.
(33) Lei, Y. M.; Zhao, M.; Wang, A.; Yu, Y. Q.; Chai, Y. Q.; Yuan, R.; Zhuo, Y. Electrochemiluminescence of Supramolecular Nanorods and Their Application in the "On-Off-On" Detection of Copper Ions. *Chem. − Eur. J.* **2016**, *22*, 8207−8214.
(34) Cheng, C.; Huang, Y.; Tian, X.; Zheng, B.; Li, Y.; Yuan, H.; Xiao, D.; Xie, S.; Choi, M. M. F. Electrogenerated Chemiluminescence Behavior of Graphite-like Carbon Nitride and Its Application in Selective Sensing Cu^{2+}. *Anal. Chem.* **2012**, *84*, 4754−4759.
(35) Hua, L.; Han, H.; Chen, H. Enhanced Electrochemiluminescence of CdTe Quantum Dots with Carbon Nanotube Film and Its Sensing of Methimazole. *Electrochim. Acta* **2009**, *54*, 1389−1394.
(36) Shen, W. J.; Zhuo, Y.; Chai, Y. Q.; Yang, Z. H.; Han, J.; Yuan, R. Enzyme-Free Electrochemical Immunosensor based on Host-Guest Nanonets Catalyzing Amplification for Procalcitonin Detection. *ACS Appl. Mater. Interfaces* **2015**, *7*, 4127−4134.
(37) Wu, J.; Chen, Y.; Yang, M.; Wang, Y.; Zhang, C.; Yang, M.; Sun, J.; Xie, M.; Jiang, X. Streptavidin-Biotin-Peroxidase Nanocomplex-Amplified Microfluidics Immunoassays for Simultaneous Detection of Inflammatory Biomarkers. *Anal. Chim. Acta* **2017**, *982*, 138−147.
(38) Li, H.; Sun, Y.; Elseviers, J.; Muyldermans, S.; Liu, S.; Wan, Y. A Nanobody-Based Electrochemiluminescent Immunosensor for Sensitive Detection of Human Procalcitonin. *Analyst* **2014**, *139*, 3718−3721.
(39) Wang, C.; Zhang, N.; Wei, D.; Feng, R.; Fan, D.; Hu, L.; Wei, Q.; Ju, H. Double Electrochemiluminescence Quenching Effects of Fe_3O_4@PDA-Cu_XO towards Self-Enhanced $Ru(bpy)_3^{2+}$ Functionalized MOFs with Hollow Structure and It Application to Procalcitonin Immunosensing. *Biosens. Bioelectron.* **2019**, *142*, 111521−111527.
(40) Yang, L.; Xue, J.; Jia, Y.; Zhang, Y.; Wu, D.; Ma, H.; Wei, Q.; Ju, H. Construction of Well-Ordered Electrochemiluminescence Sensing Interface Using Peptide-Based Specific Antibody Immobilizer and N-(aminobutyl)-N-(ethylisoluminol) Functionalized Ferritin as Signal Indicator for Procalcitonin Analysis. *Biosens. Bioelectron.* **2019**, *142*, 111562−111568.

https://dx.doi.org/10.1021/acsami.9b23248
ACS Appl. Mater. Interfaces 2020, 12, 9098−9106